


AUTHOR QUERY FORM

	Journal: YJCIS Article Number: 18890	Please e-mail or fax your responses and any corrections to: E-mail: corrections.essd@elsevier.sps.co.in Fax: +31 2048 52799
---	---	---

Dear Author,

Please check your proof carefully and mark all corrections at the appropriate place in the proof (e.g., by using on-screen annotation in the PDF file) or compile them in a separate list. Note: if you opt to annotate the file with software other than Adobe Reader then please also highlight the appropriate place in the PDF file. To ensure fast publication of your paper please return your corrections within 48 hours.

For correction or revision of any artwork, please consult <http://www.elsevier.com/artworkinstructions>.

Any queries or remarks that have arisen during the processing of your manuscript are listed below and highlighted by flags in the proof. Click on the 'Q' link to go to the location in the proof.

Location in article	Query / Remark: click on the Q link to go Please insert your reply or correction at the corresponding line in the proof
Q1 Q2	<p>Please confirm that given names and surnames have been identified correctly.</p> <p>Please note that as Refs. [34] and [56] were identical, the latter has been removed from reference list and ensuing references have been renumbered.</p> <div data-bbox="416 1853 981 1953"><p>Please check this box if you have no corrections to make to the PDF file</p><input data-bbox="868 1868 940 1932" type="checkbox"/></div>

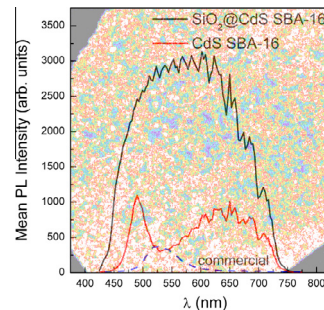
Thank you for your assistance.

Graphical abstract

White-light photoluminescence and photoactivation in cadmium sulfide embedded in mesoporous silicon dioxide templates studied by confocal laser scanning microscopy

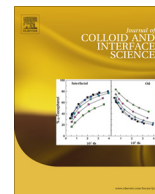
E. Pellicer^{*}, E. Rossinyol, M. Rosado, M. Guerrero, R. Domingo-Roca, S. Suriñach, O. Castell, M.D. Baró, M. Roldan^{*}, J. Sort^{*}

Journal of Colloid and Interface Science xxx (2013) xxx



Highlights

- Cadmium sulfide (CdS) embedded into SBA-15 and SBA-16 mesoporous silica templates.
- Cadmium thioglycolate precursor as a source of mesoporous CdS.
- Broad photoluminescence (PL) over the entire visible range and enhanced PL intensity.
- SiO₂@CdS composites undergo photoactivation under continuous UV illumination.



White-light photoluminescence and photoactivation in cadmium sulfide embedded in mesoporous silicon dioxide templates studied by confocal laser scanning microscopy

E. Pellicer^{a,*}, E. Rossinyol^b, M. Rosado^b, M. Guerrero^a, R. Domingo-Roca^a, S. Suriñach^a, O. Castell^b, M.D. Baró^a, M. Roldan^{b,*}, J. Sort^{c,*}

^a Departament de Física, Universitat Autònoma de Barcelona, E-08193 Bellaterra, Spain

^b Servei de Microscòpia, Universitat Autònoma de Barcelona, E-08193 Bellaterra, Spain

^c Institució Catalana de Recerca i Estudis Avançats (ICREA) and Departament de Física, Universitat Autònoma de Barcelona, E-08193 Bellaterra, Spain

ARTICLE INFO

Article history:

Received 3 February 2013

Accepted 11 June 2013

Available online xxxx

Keywords:

Confocal laser scanning microscopy

White-light photoluminescence

Photoactivation

Mesoporous silica

CdS

Nanocasting

SBA-15

SBA-16

ABSTRACT

SBA-15 and SBA-16 silica templates have been infiltrated with CdS by means of nanocasting using a hybrid precursor. The morphology and structure of both the SiO₂@CdS nanocomposites and the silica-free CdS replicas have been characterized. The three-dimensional nanocrystalline CdS networks embedded in SBA-15 and SBA-16 silica templates exhibit broad photoluminescence (PL) spectra over the entire visible range, together with enhanced PL intensity compared to silica-free CdS replicas. These effects result from the role silica plays in passivating the surface of the CdS mesostructures. Furthermore, photoactivation is eventually observed during continuous illumination because of both structural and chemical surface modifications. Owing to this combination of properties, these materials could be appealing for solid-state lighting, where ultra-bright near-white PL emission is indispensable.

© 2013 Published by Elsevier Inc.

1. Introduction

Wide band gap II–VI semiconductor nanoparticles, also termed “quantum dots (QDs)” (e.g., CdS, CdSe, ZnSe, etc.), have received considerable attention in recent years owing to their unique size-dependent optical properties that result from the quantum confinement of electron–hole pairs in the three spatial dimensions. As the nanocrystal size is reduced, the band gap increases and, consequently, a blue-shift of the photoluminescence (PL) emission is observed. This makes it possible to tune the emission color of QDs [1,2]. These materials have been proposed for a wide variety of technological applications, including biological labeling, electronic devices, optically-driven lasers and waveguides, hydrogen production, solar cells, quantum computing and solid state lighting (SSL), among others [1,3–6].

SSL devices based on QDs incorporated into light emitting diodes (LEDs) are more efficient than conventional incandescent and fluorescent lamps in aspects like mechanical stability against vibration and shock, overall life-time and, most importantly, overall power consumption [7]. Indeed, incandescent light is highly inefficient because about 90% of the energy input is emitted as heat. Hence, switching from conventional light sources to SSL would represent a massive energy saving of more than 50% [6,8]. Both organic [9] and inorganic [10] materials have been proposed for highly-efficient SSL. In terms of optical properties, SSL needs a broad-band luminescence in the wavelength interval ranging from 400 nm to 750 nm. This broad spectrum can, in principle, be obtained by simply mixing QD nanoparticles with narrow emission bands at the red, green and blue wavelengths [11], but this is not very efficient due to self-absorption effects. Alternatively, white-light emission has been reported for the so-called “magic sized” CdSe QDs, which consist of uncoated nanoparticles of about 1.5 nm in diameter [6]. To achieve the desired effects, precise control of the CdS particle size was required using specific pyrolysis techniques.

One of the drawbacks of CdS comes from the acute toxicity of Cd, which precludes its use in biomedicine and other applications. In addition, the presence of structural defects at the surface of QDs

* Corresponding authors. Fax: +34 93 5812155 (E. Pellicer), +34 93 5811845 (M. Roldan), +34 93 5812155 (J. Sort).

E-mail addresses: Eva.Pellicer@uab.cat (E. Pellicer), Emma.Rossinyol@uab.cat (E. Rossinyol), marcos.rosado.iglesias@gmail.com (M. Rosado), Miguel.Guerrero@uab.cat (M. Guerrero), roger.domingor@e-campus.uab.cat (R. Domingo-Roca), Santiago.Surinyach@uab.cat (S. Suriñach), Onofre.Castell@uab.cat (O. Castell), Dolors.Baró@uab.cat (M.D. Baró), Monica.Roldan@uab.cat (M. Roldan), Jordi.Sort@uab.cat (J. Sort).

typically causes non-radiative decay of excitons and a concomitant loss of PL. For these reasons, organic ligands are commonly used to coat and passivate the surface of QDs [12,13]. However, these ligands make the QDs hydrophobic, while most biological applications require water-soluble systems. Alternatively, QDs can be embedded into silica colloids or inside silica mesostructures, which are biocompatible [14–16]. Coating QDs with silica also leads to effective surface passivation and enhances the PL intensity [17,18].

Furthermore, the PL intensity can sometimes be enhanced by illuminating the QDs with UV or visible light. This phenomenon is known as photoactivation [14,19–23], and can be fostered in the presence of certain liquids or gases that facilitate passivating the QD surface in a reversible or irreversible manner. Photoactivation competes with an opposing effect called photobleaching, which is the decrease in the PL intensity due to photon-induced chemical damage and concomitant increase of non-radiative decay [24].

Besides nanoparticles, one-dimensional semiconductor nanostructures with variable geometry (e.g., nanowires, nanotubes, nanobelts and nanohelices) also maintain the interesting luminescent properties that arise from quantum confinement effects [25–27]. When arranged in the form of 2D or 3D periodic structures (for example, in ordered mesoporous frameworks), these materials can be regarded as a negative replica of an array of regularly-spaced QDs. Therefore, these arrangements are often referred to as “quantum antidots” [28,29]. Similar to QDs, it should be possible to tune the band gap of quantum antidots to meet specific technological demands [29]. Actually, some functionalities of QDs that depend on the overall surface area (e.g., photocatalysis, photovoltaic activity and electrochemical properties) would presumably be enhanced in mesoporous quantum antidots [25,30].

So far, reports on mesoporous 2D or 3D CdS structures have been rather scarce [31–39]. In fact, although there is extensive literature on the synthesis of CdS nanoparticles with a narrow size distribution, the rational design of mesoporous 3D CdS architectures is still in its infancy. The first report on the preparation of mesoporous CdS (2D hexagonal superlattices) dates from 1996, when the soft-templating method was used to prepare these materials from an organic phase consisting of tubules of self-assembled amphiphiles [31]. CdS superlattices have also been obtained by direct templating in a lyotropic organic liquid crystal [32]. Similarly, CdS aerogels with thick walls have been produced by assembling nanoparticles [33]. In turn, mesoporous CdS with disordered pore arrangements have been obtained using template-free ultrasonic mediated precipitation [34]. All these processing routes suffer from the drawback that either they render non-crystalline CdS structures with poor optical properties, or the pore distribution is rather inhomogeneous both in size and lateral spacing.

Interest in the use of hosts to accommodate CdS within their pore networks started with zeolites two decades ago, triggered by the early works of Herron and Stucky [35,36]. Later, the use of mesoporous silicas to accommodate CdS in their interior and the possibility to selectively etch away the SiO₂ to obtain self-supported CdS replicas has attracted attention. Nevertheless, there are still very few works on the nanocasting synthesis of 3D mesoporous CdS using silica mesostructures as a hard template [37]. Since SiO₂ can stand calcination at relatively high temperatures, the degree of crystallinity in nanocast CdS is usually higher than in soft-templating routes, and therefore better optical performance is attained. However, due to the low yield and poor pore filling, it is a challenge to form truly ordered mesostructured networks and only isolated dispersed nanoparticles are generally obtained inside the mesopores of the hard templates [38–41]. In most cases the CdS nanoparticles have been introduced in mesoporous silica via reverse micellar systems [42,43].

Higher filling of mesoporous silica hosts with CdS has been achieved by using a special lab-made hybrid precursor, cadmium thioglycolate (Cd₁₀S₁₆C₃₂H₈₀N₄O₂₈) [44], or by one-step impregnation method to replicate mesoporous CdS using thiourea [45]. Hexagonally-packed arrays of CdS and Cd_{1-x}Mn_xS nanowires have also been synthesized from Cd xanthate and a mixture of Cd and Mn acetates, respectively, using mesoporous silica as a hard template [46,47]. In all these studies, either the SBA-15 or the MCM-41 silica mesostructures were the matrices utilized. Hence, the geometry of the semiconductor obtained was essentially limited to interconnected nanowires. Furthermore, these previous works mainly focused on the synthesis and structural characterization of the obtained replicas, while the possible benefits for the PL properties of hosting 3D quantum antidots inside the pores of mesoporous silica were largely overlooked.

In this work we report on the synthesis of CdS quantum antidots inside the pores of SBA-15 (hexagonally-arranged cylindrical pores) and SBA-16 (interconnected spherical cages) mesoporous silica templates, using cadmium thioglycolate as precursor. Although the confocal laser scanning microscope (CLSM) is mostly (and traditionally) used in the biology field, it is here applied to study the PL properties of the synthesized materials to simultaneously explore its potential in material science [48,49]. On comparing the PL spectra of SiO₂@CdS composites and SiO₂-free CdS mesoporous frameworks, it rapidly emerges that the synthesized materials exhibit an interesting range of photoemission properties. The extremely different responses encountered in absorption, PL emission, and photoactivation experiments are linked to both the presence/absence of the silica hosts and the type of mesostructure arrangement (SBA-15 and SBA-16). In particular, the presence of the SiO₂ template results in a pronounced enhancement of the PL and broad white-light emission spectra.

2. Materials and methods

2.1. Synthesis of cadmium thioglycolate, [Cd₁₀(SCH₂CH₂OH)₁₆](NO₃)₄, precursor

The cadmium thioglycolate precursor was synthesized following the procedure described in [50]. In brief, 6.12 g of Cd(NO₃)₂ was dissolved in 100 mL of dry THF in a 250 mL round-bottomed flask under argon atmosphere. While stirring, 3.12 g of mercaptoethanol dissolved in 50 mL of dry THF was injected with a syringe through a silicon rubber septum into the flask at room temperature. When the addition was complete, the mixture was stirred at reflux for 24 h ($T \sim 65^\circ\text{C}$) by which time a white precipitate appeared. The reaction mixture was then first cooled to room temperature, left in the fridge overnight, and finally the whitish precipitate was filtered off. The solid was washed several times with excess amounts of diethyl ether, and the resultant white powder was collected and dried under vacuum.

2.2. Synthesis of silica templates

SBA-15 silica was synthesized by dissolving 6.0 g Pluronic P123 copolymer in 225 g diluted HCl (1.35 M). 12.5 g of tetraethyl ortosilicate (TEOS, from Sigma-Aldrich), which served as the silicon source, was then added and the solution stirred for 24 h at a constant temperature (about 37 °C) [51]. The hydrothermal treatment was carried out at 90 °C in a sealed plastic container for 24 h. The solid obtained was filtered, washed copiously with water and finally calcined at 550 °C for 5 h to remove the organics. A scan rate of 1 °C min⁻¹ was used to raise the temperature from room temperature to 550 °C. SBA-16 silica was synthesized under similar conditions by using Pluronic F127 (EO₁₀₆PO₂₀EO₁₀₆) as the surfac-

tant. In this case, 6.0 g of F127 was dissolved in 180 g diluted HCl and 6.6 g KCl salt [51].

2.3. Synthesis of CdS@SiO₂ composites and silica-free CdS replicas

For the impregnation of silica templates, 0.026 g of silica powder (SBA-15 or SBA-16) was placed in contact with 0.128 g of cadmium thioglycolate dissolved in 15 mL of water. The mixture was stirred for 30 min in a crucible and left for water evaporation overnight. The solid was then first heated up to 120 °C at a rate of 1 °C/min, held at this temperature for 10 h, and thereafter up to 160 °C and left at this temperature for 24 h. At the end of the heating process, the furnace was slowly cooled down to room temperature. The yellow solid obtained consisted of CdS embedded into SiO₂ templates (SiO₂@CdS composites). The silica hosts were selectively etched with 2 M NaOH solution at 70 °C under stirring for 24 h. The released CdS powder was collected after centrifugation and the supernatant was decanted off, copiously rinsed in ethanol and finally dried.

For comparison, CdS uncapped nanoparticles were purchased from Aldrich (98% purity powder). The structure and properties of these particles were compared with those of the CdS mesostructures.

2.4. Structural characterization using scanning and transmission electron microscopies and X-ray diffraction

Scanning electron microscopy (SEM) images were acquired on a Zeiss Merlin microscope operated at 1.20 kV. Transmission electron microscopy (TEM) analyses were carried out on a Jeol-JEM 2011 microscope operated at 200 kV. Samples for TEM observation were prepared by dispersing a small amount of powder in ethanol and then one or two drops of the suspension were placed dropwise onto a holey carbon supported grid. Energy dispersive X-ray spectroscopy (EDX) was used for elemental analysis of the powders. The nitrogen adsorption–desorption isotherm measurement was performed on a Micromeritics ASAP 2020 accelerated surface area and porosimetry analyzer at the temperature of liquid N₂ (77 K). The Barrett–Joyner–Halenda (BJH) approach was applied to determine the pore size distribution and average pore diameter by using adsorption data of the isotherms.

The structure and phase percentages of the powders were studied by X-ray diffraction (XRD), using Cu K α radiation, in the Bragg–Brentano geometry operating in the step scan mode. Microstructural parameters (phase percentages, cell parameters, crystallite sizes and microstrains) were quantified from the XRD patterns by means of a data analysis program based on a full pattern fitting procedure (Rietveld method) [52]. The effects of preferred orientation on the patterns were also taken into account in the calculations.

2.5. Absorbance measurements and photoluminescence studies using confocal laser scanning microscopy

Absorbance measurements were performed using a Hewlett–Packard 8453 UV–Vis spectrophotometer in the wavelength range between 300 and 800 nm. The photoluminescence spectra of CdS samples were determined using a wavelength (λ)-scan function of confocal laser scanning microscopy (CLSM), based on a fluorescence method that displays the complete spectral distribution of the fluorescence signals. The CdS powders were mounted on Mat-Teck culture dishes (Mat Teck Corp., Ashland, Massachusetts, United States). Images were acquired with a CLSM Leica TCS-SP5 AOBS spectral microscope (Leica Microsystems Heidelberg GmbH; Mannheim, Germany) using a Plan-Apochromat 63X objective (NA 1.4, oil). Series of images ($xy\lambda$) were taken to determine the spectra

emissions of the samples and to establish their maxima. Intrinsic fluorescence was excited with a 405 nm line of a blue diode laser and the Acousto-Optic Tunable Filter (AOTF) was set at 70%. Fluorescence emission was collected with a hybrid detector in 5 nm bandwidth increments (λ step size = 3 nm) in the range from 425 nm to 775 nm. The images were captured in 512 \times 512 pixels with 12 bits of dynamic range. A silica spectrum was collected as a negative control. A Region of Interest (ROI) was defined to determine the mean fluorescence intensity (MFI) in the selected area in relation to the emission wavelength. A set of 10 ROIs of 15 μ m² was used to analyze the mean fluorescence intensity and the maximum emission range of the samples. Fluorescence measurements are expressed in arbitrary units (a.u.) but were all acquired under the same imaging conditions.

Photostability experiments were performed in air using the Live Data Mode function of the CLSM, which makes it possible to monitor long time-lapse experiments. A 50 mW blue diode 405 nm laser was used at a fairly high output (AOTF = 90%) to target small regions (24 μ m², zoom = 10). Images were taken at 2.5 s intervals during 10 min, in 512 \times 512 pixels with 8 bits of dynamic range. In the area where the laser was at its maximum illumination power, 5 ROIs of 15 μ m² were selected to show the MFI in the region in relation to time. For the irreversibility studies, the samples were irradiated during 5 min with a mercury-halide UV lamp (120 W, exciting wavelength in the range 300–600 nm). Data from all studies were analyzed using the LAS AF software ver. 2.4.1. (Leica Microsystems).

3. Results

High-resolution SEM (HRSEM) images of the silica templates, shown in Fig. 1a and d, reveal the typical pore geometry of the SBA-15 and SBA-16 mesostructures. While the SBA-15 host consists of hexagonal arrays of high-aspect ratio channels (Fig. 1a), the SBA-16 template is composed of cubic arrangements of spherical nanocavities (Fig. 1d). The average pore diameter is around 7 nm for the SBA-15 template and 4 nm for the SBA-16 template, as shown in the TEM images included as insets.

Fig. 1b shows a TEM image of CdS-filled SBA-15 silica template (SiO₂@CdS SBA-15 composite). Note that the channels that are filled with CdS give a darker contrast in the bright-field image (Fig. 1b) because of the higher atomic number of Cd, while the channels that remain unfilled look brighter. All the silica voids imaged by TEM appear to be occupied to a large extent by CdS. Upon removal of the silica template, nanowire arrays typical of the SBA-15 mesostructure are observed at low magnification (inset in Fig. 1b). High-resolution TEM (HRTEM) images reveal that each of the CdS nanowires actually consists of a chain of crystalline nanoparticles, as shown in Fig. 1c. The average diameter of the nanowires is 7–8 nm, which matches the pore size of the parent host.

Due to the relatively large thickness of the SBA-16 silica particles, TEM observations of the CdS-filled mesostructure (SiO₂@CdS SBA-16 composite) are more challenging. Nevertheless, the porous structure can still be seen at the outer regions of the mesoporous particles (see Fig. 1e). In this case, because of the particular pore topology of SBA-16 silica, the presence of CdS embedded in the spherical nanocavities is more difficult to prove, although pseudo-ordered arrays of CdS nanoparticles can still be seen after the silica template has been removed (inset in Fig. 1e). The corresponding EDX spectra, acquired from several particles, confirm the presence of Cd and S together with the peaks from the silica matrix (Si and O) (see Supporting Information Fig. S1). The HRTEM images of silica-free CdS nanoparticles reveal crystallite sizes around 5 nm with well-defined lattice fringes, again confirming

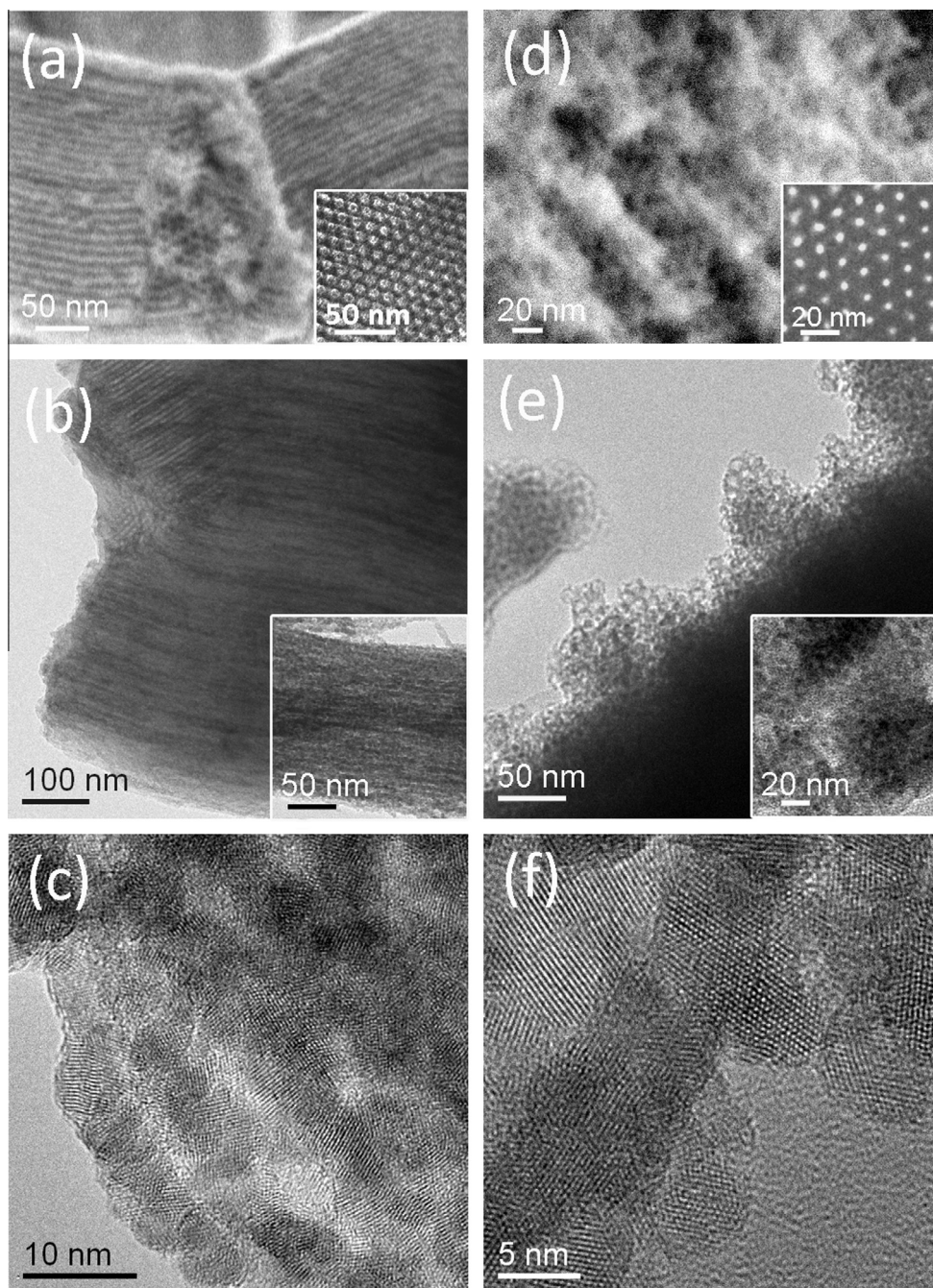


Fig. 1. (a and d) HRSEM images of SBA-15 and SBA-16 silica hosts, respectively. A detail of the pore topology is shown in the inset TEM images. (b and e) TEM images of SiO₂@CdS SBA-15 and SBA-16 composites. The insets show a TEM image of the corresponding silica-free CdS powders (replicas). (c and f) HRTEM images of silica-free SBA-15 and SBA-16 CdS powders. Note that the TEM images in panels (a and d) correspond to the porous structure of the SBA-15 silica along the [100] and SBA-16 silica along the [111] zone axes, respectively.

the crystalline nature of the CdS replica (Fig. 1f). A sketch of the geometry of the different samples (SiO₂ host, SiO₂@CdS and silica-free CdS) is shown in Fig. 2.

It is noteworthy that CdS crystals were not found outside the silica hosts for both SiO₂@CdS SBA-15 and SBA-16 composite powders, suggesting that the hybrid precursor entered the silica mesochannels completely during the impregnation step. To prove this, N₂ adsorption-desorption measurements of the SiO₂ hosts and of the SiO₂@CdS composites were carried out (Fig. 3). The BET surface area of SBA-15 SiO₂ decreased from 602.8 m² g⁻¹ to 53.7 m² g⁻¹ after CdS was loaded, thus proving the successful filling of the silica pores with CdS to a great extent. Similarly, the

BET surface area of SBA-16 SiO₂ decreased from 280.3 m² g⁻¹ to 30.0 m² g⁻¹ after CdS was loaded. The corresponding pore size distributions are shown in the insets. The mean pore size determined from the adsorption branch is 6.6 nm for SBA-15 SiO₂ and 4.8 nm for SBA-16 SiO₂. The pore sizes of the corresponding SiO₂@CdS composites were maintained, indicating that part of the pores of the silica hosts remained empty after the formation of CdS from the cadmium thioglycolate precursor [53]. No interparticle porosity attributable to CdS outside the silica hosts is observed for the SiO₂@CdS composites, again confirming that CdS entered the silica channels. After removal of silica templates, a Cd:S ratio close to 1 is obtained, as evidenced by EDX analyses (Supporting Information

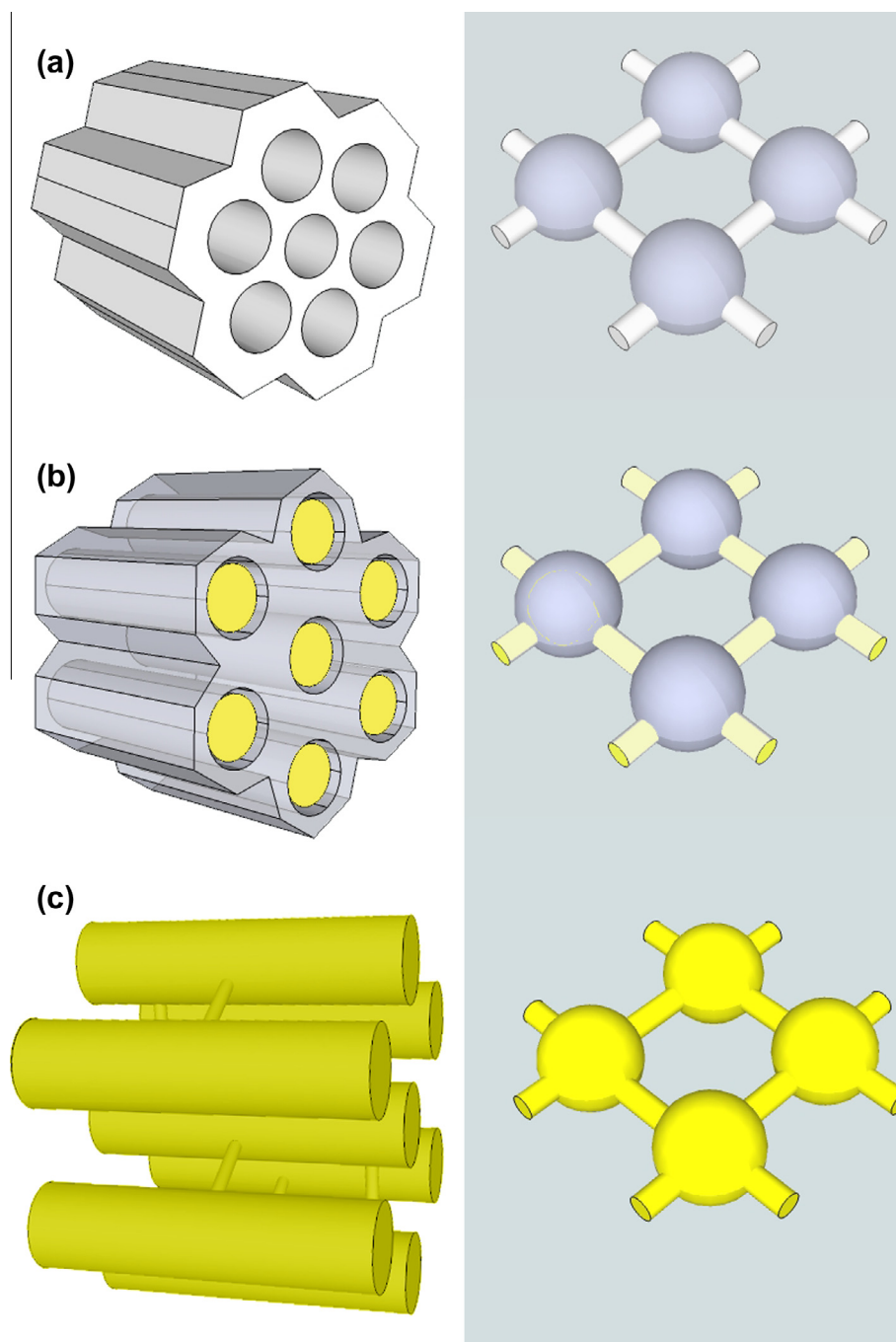


Fig. 2. Schematic drawings of (a) SiO₂ template, (b) SiO₂@CdS composite and (c) silica-free CdS sample geometries for SBA-15 type (left) and SBA-16 type (right).

Fig. S1). Moreover, no traces of silicon are detected, which confirms that the SiO₂ was successfully removed during the etching step.

The XRD patterns of the CdS mesoporous replicas, obtained after removal of SBA-15 and SBA-16 templates, are shown in Fig. 4. For the aim of comparison, the pattern corresponding to commercial CdS nanoparticles is also shown. All samples consist of a mixture of wurtzite (hexagonal close-packed) and zinc-blende (cubic) phases, whose Miller indices are indicated in the figure. Both hexagonal and cubic phases are known to be highly photoluminescent [54]. The XRD peaks are rather broad, suggesting that the coherently diffracting length (i.e., crystallite size) falls within the nm range. Rietveld refinements of the XRD patterns reveal that the mesoporous CdS frameworks are rich in wurtzite phase

(around 80 and 62 vol.% for the SBA-16 and SBA-15, respectively), whereas the zinc-blende content in the commercial CdS powders is around 43% (see Table 1). The crystallite size is around 6 nm for both CdS SBA-15 and SBA-16 and 13 nm for the commercial powder. The values of microstrains are relatively small ($<10^{-4}$) in all cases. The crystallite size is in rather good agreement with the pore size of the parent silica hosts, as determined from TEM and BET analyses.

Fig. 5 shows the absorbance spectra of the different investigated samples. A peak is observed around 500 nm for the commercial particles, close to the position of the first excitonic transition expected for bulk CdS (512 nm) [55]. This peak shifts towards lower λ values (i.e., blue-shift) in both mesoporous silica-free CdS and

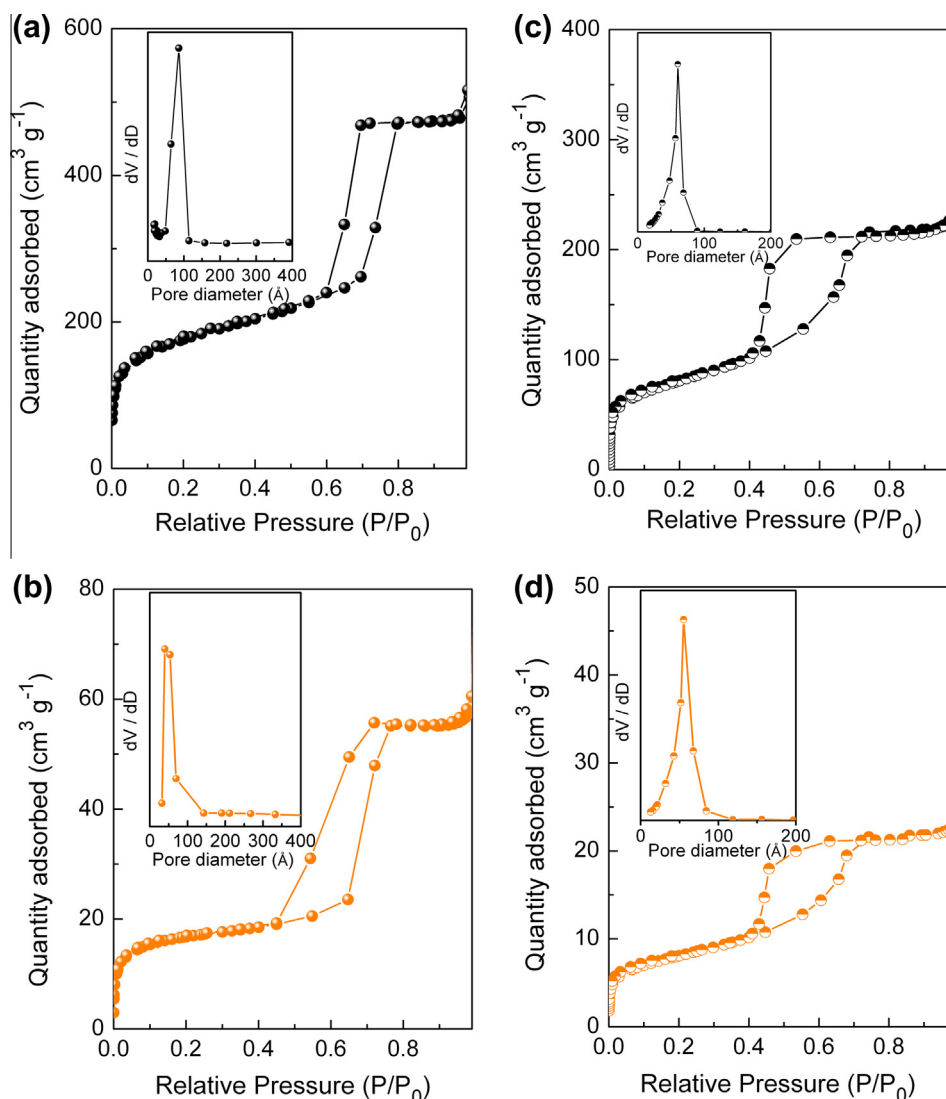


Fig. 3. N₂ adsorption–desorption isotherms for (a) SiO₂ SBA-15 template, (b) SiO₂@CdS SBA-15 composite, (c) SiO₂ SBA-16 template and (d) SiO₂@CdS SBA-16 composite. The corresponding pore size distributions are shown as insets.

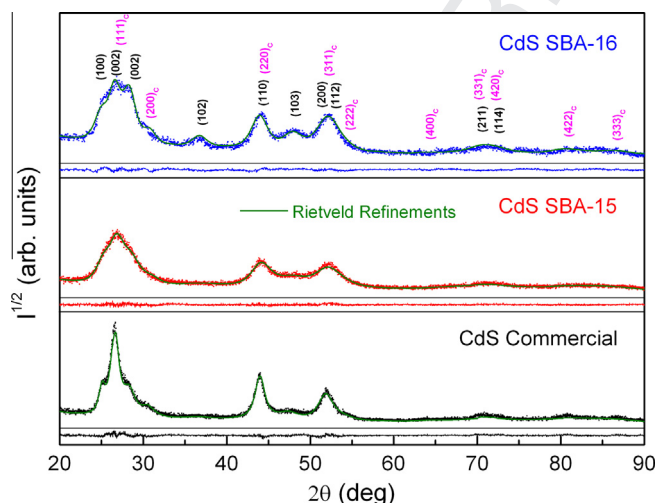


Fig. 4. Experimental (scattering) and computed (solid line) X-ray diffraction patterns of silica-free CdS SBA-15 and SBA-16 powders and commercial CdS particles. For each sample, the difference between the experimental and Rietveld-fitted profiles is shown at the bottom.

SiO₂@CdS composite samples. The peak broadening observed in the latter (particularly pronounced for SBA-15) could be due to light scattering from the presence of SiO₂, as similarly observed in other coated or embedded quantum dots [34]. The shift towards lower λ values is attributed to the decrease in the crystallite size, in agreement with other works from the literature [55,56]. Although the crystallite sizes in CdS SBA-15 and SBA-16 are very similar, the shift in absorbance is more pronounced for SBA-16. This is probably because the geometry of the two mesoporous structures is different: the SBA-15 consists of chain-like interconnected CdS nanocrystals, whereas in the SBA-16 the nanocrystals are better isolated from each other and quantum effects are probably exacerbated.

The photoluminescence spectra of the SBA-15 and SBA-16 CdS mesostructures, with and without the presence of the SiO₂ matrix, are shown in Fig. 6, together with confocal microscopy images of the illuminated particles at the emission wavelength corresponding to maximum intensity. The PL spectra of the silica-free CdS frameworks have two peaks: a band edge emission centered around 480 nm and a broad band centered around 650 nm, which corresponds to the deep trapped fluorescence emission arising from surface states, i.e., light emitted when a photogenerated hole,

Table 1

Summary of the microstructural parameters (i.e., wurtzite/zinc blende volume phase percentages, crystallite sizes ($\langle D \rangle$) and microstrains ($\langle \epsilon^2 \rangle^{1/2}$), as determined from Rietveld refinements of the XRD patterns of the silica-free SBA-15 and SBA-16 CdS mesoporous materials and for the commercial powder.

	% vol. Wurtzite	$\langle D \rangle_{\text{Wurt}}$	$\langle \epsilon^2 \rangle^{1/2}_{\text{Wurt}}$	% vol. Zinc Blende	$\langle D \rangle_{\text{ZB}}$
CdS SBA-16	80	6	0.0001	20	7
CdS SBA-15	62	5	0.0006	38	7
CdS Commercial	57	12	0.0003	43	14

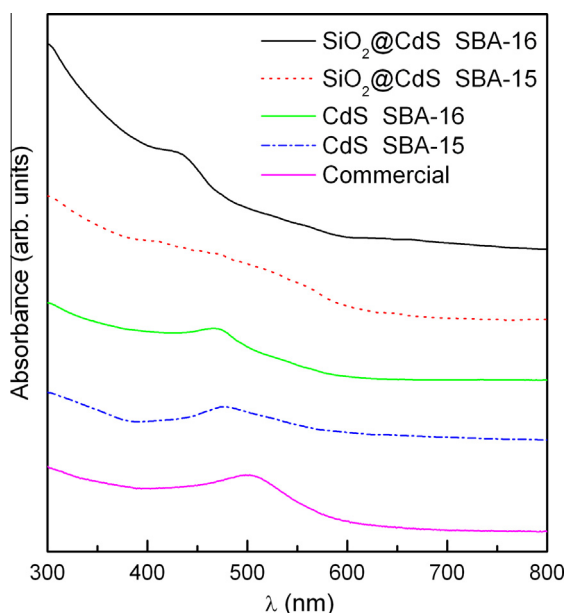


Fig. 5. UV-Vis absorption spectra for: SiO₂@CdS SBA-15 and SBA-16 composites, the corresponding silica-free CdS materials, and the commercial powder.

trapped in a midgap state, encounters an electron before it can relax non-radiatively to the ground state [2]. Remarkably, a single broad-band emission is obtained in the SiO₂@CdS mesoporous composites, and covers the entire visible range (in the wavelength interval 420–750 nm). In all mesoporous materials herein investigated, there is a large Stokes' shift between the absorbance and emission peaks, i.e., the emitted light is of lower energy than the excitation light. Such a difference stems from the non-radiative relaxation being lost as thermal decay.

Besides the rather large width, there are several other additional features of the PL spectra in Fig. 6 that are worth mentioning. First, the band emission peak of the commercial particles is located at a longer wavelength than those of the mesoporous CdS. The blue-shift of the PL spectra in the mesoporous CdS is due to its smaller crystallite size compared to the commercial CdS (see Table 1), since the separation between electron and hole levels is known to increase when particle size decreases [57]. Furthermore, enhanced PL is obtained when the CdS networks are embedded inside the pores of the mesoporous SiO₂ (i.e., before template removal). This is already very obvious from the confocal microscopy images and is typical in systems where the semiconductor QDs are encapsulated inside semiconductor materials with a wider band gap or electric insulators (e.g., core-shell dots) [17,18,58]. The irregular surface states due to abrupt termination of atoms coordination generally act as electrons or hole traps, leading to energy levels within the energy gap of the semiconductor nanoparticles and concomitant non-radiative recombination transitions [1]. Surface treatments aimed at passivating the nanoparticles with shells of a material with a larger band gap tend to enhance the quantum yield since this process favors the bonding of surface atoms with

the neighboring material, thus eliminating all the energy levels inside the gaps and confining electron-hole pairs to the interior of the crystals [59].

It is interesting to note that the PL spectra of the samples (with and without silica) exhibit a multi-peak structure. This oscillatory behavior is not observed in the commercial CdS particles. Remarkably, these discrete PL peaks are located at the same λ position (i.e., they have the same energy) when independent spectra are acquired from different regions of the sample, as shown in Fig. S2 (Supporting Information), thus ruling out the possibility that the sharp features are noise-induced artifacts. Furthermore, these oscillations in the PL intensity are also clearly seen in the PL scans acquired at progressively longer wavelength values (see the video in Supporting Information S3). Discrete PL spectra have been reported in other porous materials, for example in Si, but usually at low temperatures [60]. The occurrence of these sharp discrete fringes has been ascribed to a variety of factors: quantization effects due to the thickness of the wires inside the porous structure [61]; interference patterns arising from the emission of the irradiated particles at different locations [62]; phonon-assisted PL processes from dot crystallites with a discrete distribution of sizes [63] and, more recently, simply using the configurational-coordinate model of energy levels applied to porous materials [60]. Although the origin of this unusual PL behavior needs to be further investigated, it is clear that the discretization of the PL spectra seems to be inherently related to the mesoporous nature of the investigated materials.

Often, particularly in organic fluorescent dots, a decrease in the PL intensity is observed during illumination with UV or visible light, a phenomenon referred to as photobleaching [21,64]. This effect, which limits the life-time and applicability of QDs, is due to the generation of surface defects with intermediate electronic states leading to non-radiative relaxation. However, under specific conditions, the opposite effect can be observed, namely a progressive increase in the PL intensity during light irradiation. This is called photoactivation [15,19,21,56]. The dependences of the PL intensity with illumination time are shown in Fig. 7 (panels (c) and (f)) for CdS SBA-15 and SBA-16, with and without the presence of silica. Interestingly, while the intensity mainly decreases for silica-free CdS SBA-15 (and for the commercial CdS), the opposite occurs in the SBA-16 mesostructures. The confocal images shown in Fig. 7a, b, d and e confirm these results. Actually, both effects (photobleaching and photoactivation) occur simultaneously in the investigated materials, as evidenced in the video shown as Supporting Information S4, in which the brightness of most of the SBA-16 CdS nanoparticles increases with illumination time but decreases in a few of them. The dependence of the PL intensity with time for SiO₂@CdS SBA-15 also suggests that there is a competition between photobleaching and photoactivation effects. That is, a slight increase in the PL signal is observed after short-term illumination but the PL further decreases for longer illumination times. Such predominance of photobleaching is not observed in SBA-16 mesostructures (both with and without silica), even after illumination times longer than 1 h.

Although the CSLM does not provide absolute PL quantum yields, the broad-band photoluminescence emission obtained from

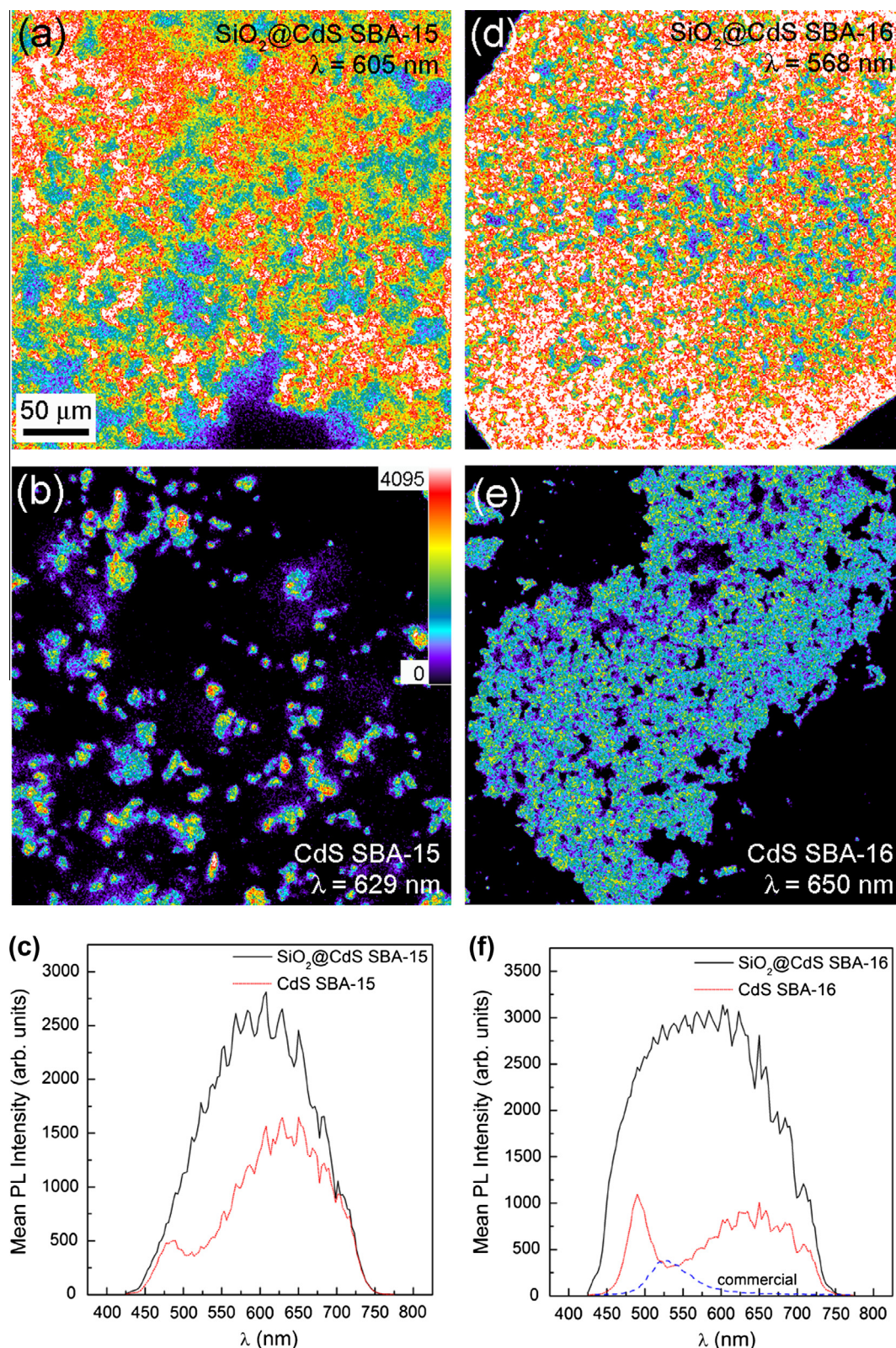


Fig. 6. CSLM images of (a and d) SiO₂@CdS SBA-15 and SBA-16 composites and (b and e) the corresponding SiO₂-free CdS replicas corresponding to the λ_{max} PL for a $\lambda_{\text{exc}} = 405$ nm. The color key is shown at the top right corner of panel (b). (c and f) Spectral profiles representing PL intensity versus emission wavelength in the 425–775 nm range. Data are the mean from $n = 10$ ROIs of the three fields examined. The profile for the commercial CdS particles is shown for comparison.

the semiconductor structures embedded in the SiO₂ templates could make these materials potentially appealing for being used in solid-state white-light emitting diode (LED) devices. These devices could become a very efficient alternative in terms of power

consumption, since their use would presumably represent important energy savings [6]. Typically, broad luminescence bands can be obtained by mixing semiconductor nanoparticles with narrow emission bands at the red, green and blue wavelengths [11], but

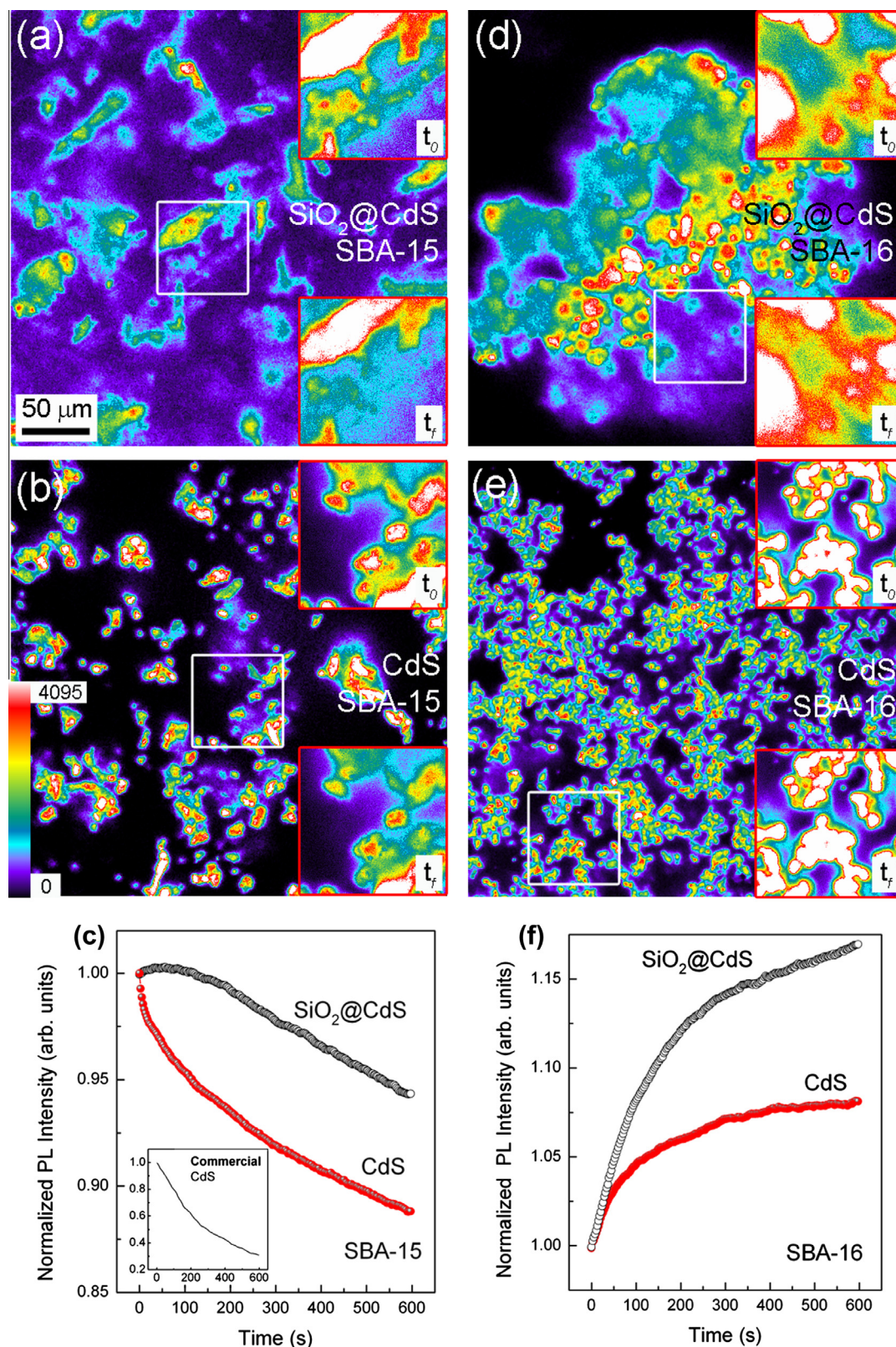


Fig. 7. CSLM images illustrating changes in the emission signal in (a and d) $\text{SiO}_2@\text{CdS}$ SBA-15 and SBA-16 composites and (b and e) the corresponding silica-free CdS materials during continuous irradiation with $\lambda_{\text{exc}} = 405$ nm laser line at maximum power. The area of interest is enclosed within the white boxes for each CSLM image. The upper and bottom insets show how the emission changes in this area of interest at the beginning ($t = 0$ min) and end ($t = 10$ min), respectively, of irradiation. The color key is shown at the bottom left corner of panel (b). (c and f) Corresponding fluorescence intensity versus time plots. The profile for the commercial CdS particles is shown for comparison.

this strategy results in an overall reduction in device efficiency due to self-absorption effects between the differently sized nanocrystals. In our case, the large Stokes' shift between the absorbance

and PL peaks ensures that the self-absorption effects are minimized. Remarkably, white light emission has also been obtained from the so-called "magic-sized" ultra-small CdS and CdSe

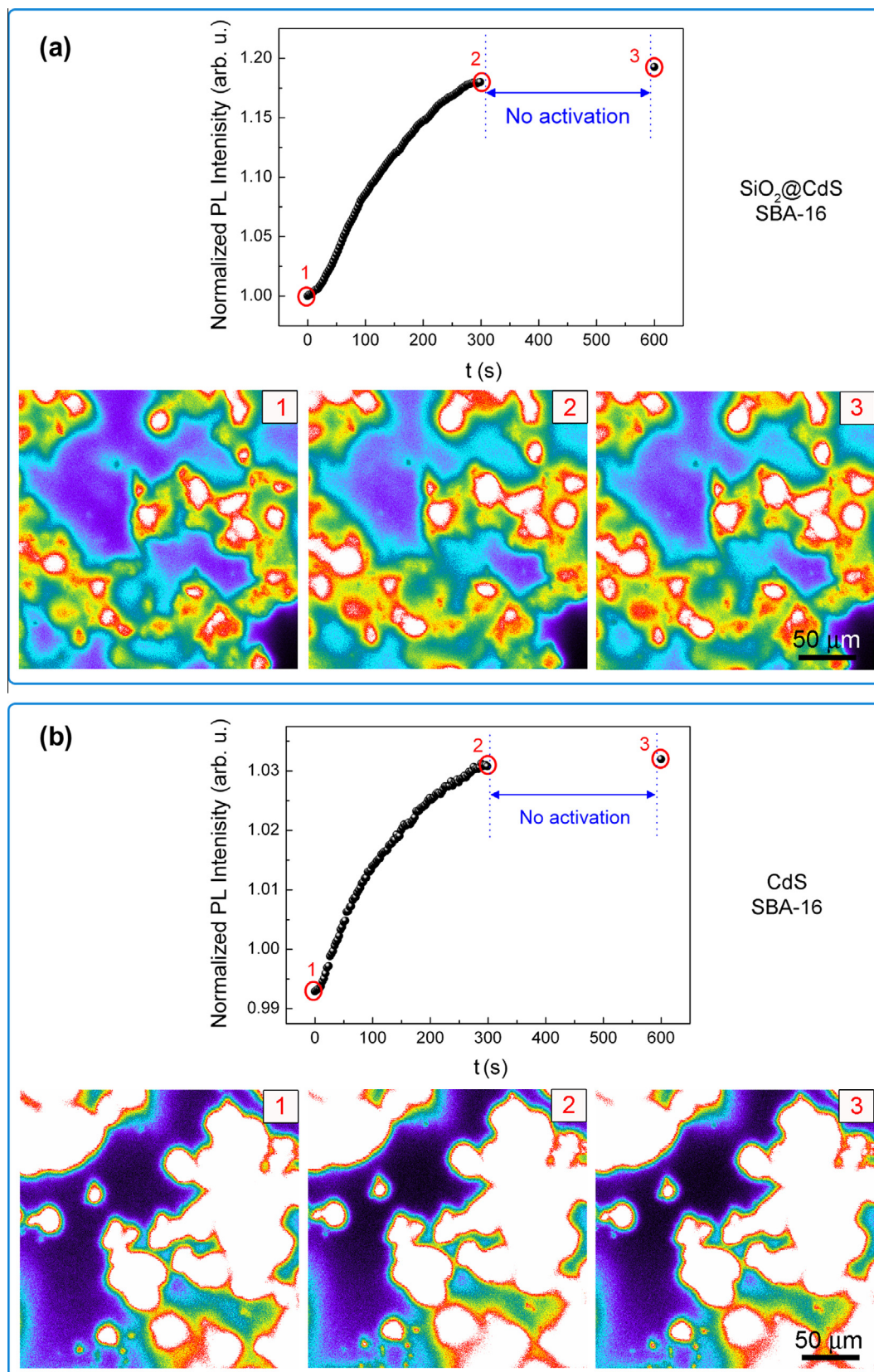


Fig. 8. PL intensity evolution with time in (a) SiO₂@CdS SBA-16 composite and (b) the corresponding silica-free CdS replica during a photoactivation experiment. Note that under continuous illumination at $\lambda_{\text{exc}} = 405$ nm for $t = 5$ min, the PL intensity increases significantly (points 1 and 2). After 5 min in dark (no activation), the PL remains the same as before (points 2 and 3), indicating that this is an irreversible process. The CSLM images taken at the indicated points in the PL versus time plot for a given area are shown at the bottom.

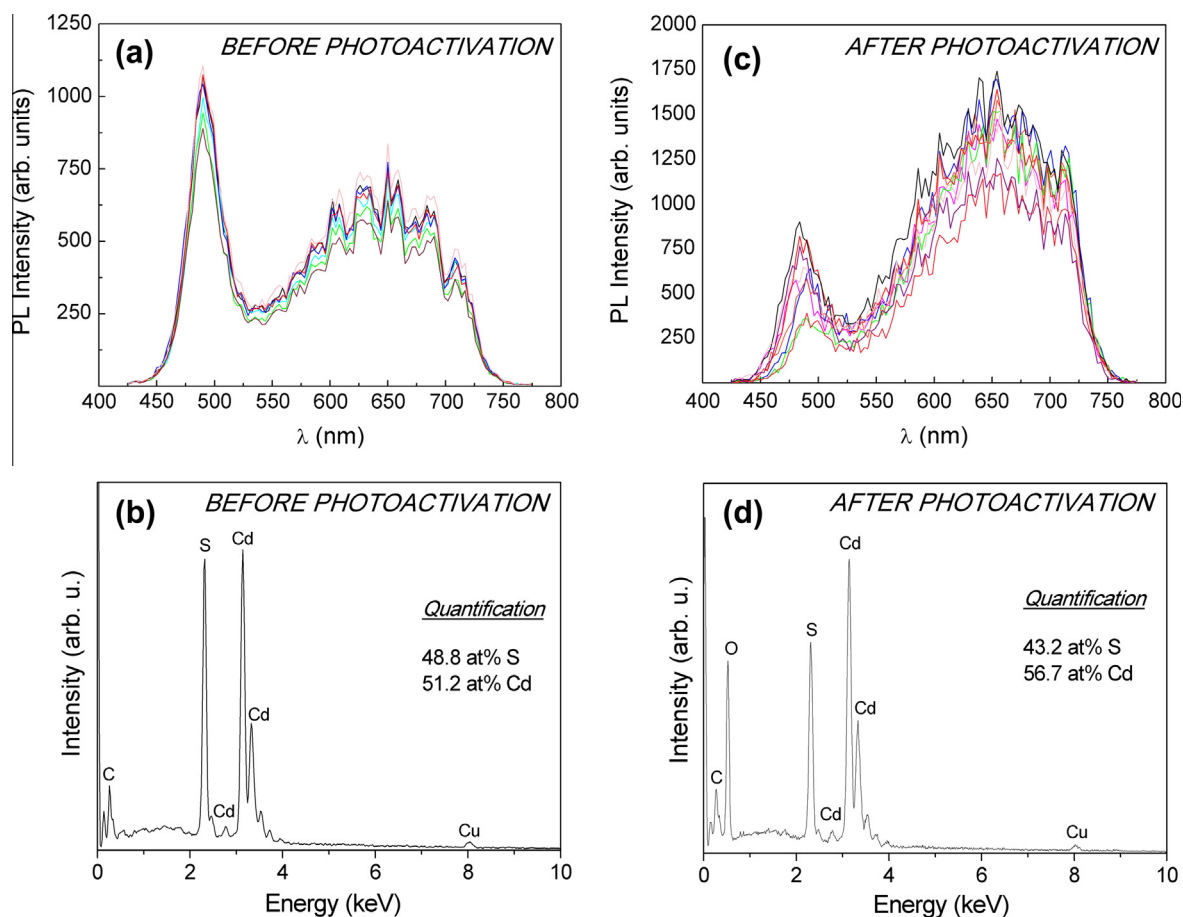


Fig. 9. Spectral profiles representing PL intensity versus emission wavelength, for several ROIs, both before (a) and after (c) photoactivating the $\text{SiO}_2\text{@CdS}$ SBA-16 composite for 1 h with the UV lamp. Panels (b) and (d) show the EDX compositional analyses before and after photoactivation, respectively.

nanoparticles, typically with sizes around 2 nm, i.e., with a large surface-to-volume ratio [6,8,12]. The generation of white light in these nanoparticles has been attributed to the recombination of charges trapped in the surface state of the semiconductor nanocrystals, in particular the recombination of an electron in the conduction band with a hole trapped in atomic vacancies near the valence band. The wide PL peak at large λ in the CdS mesostructures, stemming from deep-trap surface states, indicates that also in this case the large surface-to-volume ratio of the mesoporous materials is responsible for the broadening of the PL spectra. The enhancement in the PL intensity that occurs in the $\text{SiO}_2\text{@CdS}$ nanocomposites is likely to be due to the effective role of silica in passivating the existing surface defects.

Similarly, the main reason for the photoactivation is presumably the light-assisted smoothing (i.e., passivation) of the CdS particles surface. Activation is found to predominate in the SBA-16 sample, where the surface-to-volume ratio is larger than for SBA-15. In the latter, the chain CdS crystallites are more interconnected and there is less surface in contact with SiO_2 or air. Stronger activation is observed in CdS embedded in the SBA-16 mesoporous silica, where the semiconductor is supposedly better shielded against photocorrosion effects. This is in agreement with some results from the literature. Namely, although a laser-induced increase in the PL intensity has been found in CdSe@CdS/ZnS core-shell nanorods, virtually no change or even a decrease in PL was observed in uncoated CdSe nanorods [65]. In addition, more effective photoactivation has been reported in silica-coated CdSe nanoparticles compared to bare QDs [58].

Photoactivation can be ascribed to a variety of factors [15,19,21,56]: (i) passivation of surface states due to the adsorp-

tion of water, oxygen or other molecules, (ii) photoelectrification/neutralization processes or (iii) surface/interface structural transformations, such as annihilation of defects. Only the latter factor is irreversible in character, while the first two are reversible in the sense that deactivation rapidly takes place once the exciting light has been switched off. Hence, to shed light on the physical origin of the observed photoactivation, the reversibility of the process was investigated by illuminating the silica-free CdS and $\text{SiO}_2\text{@CdS}$ SBA-16 mesostructures with the UV lamp for 5 min, then interrupting the illumination for 5 min and subsequently switching the light on again, in order to probe possible changes in the PL intensity. The results reveal that no loss of the PL intensity occurred during the time the sample was kept in the dark (see Fig. 8).

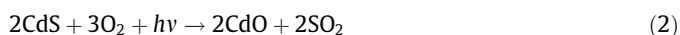
Fig. 9a and b shows the PL scans obtained at different regions of the samples before and after photoactivation for 1 h. Interestingly, while no pronounced blue-shift was observed in the band-edge PL peak, the deep-trap broad hump located at a higher λ significantly increases in intensity after UV illumination, thus suggesting that the irreversible structural changes occur mainly at the surface of the particles.

Furthermore, the PL spectra after photoactivation are slightly different depending on the region imaged, which is in agreement with the idea that not all particles undergo the same structural changes as light irradiation proceeds (as suggested by the video shown in Supporting Information S4). In particular, slight shifts in the position of the band-edge peak are observed and the wavelength positions of the discrete PL peaks also vary for the different particles, which indicate that topological changes probably occur at the particles' surface during irradiation.

Interestingly, EDX analyses performed before and after photo-activation (see Fig. 9c and d) reveal that the amount of Cd increases at the expense of the S content. Therefore, a photo-induced chemical reaction is likely to occur. It is known that CdS may be decomposed if exposed to light in the presence of oxygen. In aqueous solutions, the following reaction has been put forward [15]:



which results from a gradual release of Cd^{2+} from the QD surface. Under dry conditions, CdS would react with oxygen to yield CdO and SO_2 , since CdO is more stable than CdS:



Thermal annealing of CdS in air has been reported to lead to sulfur vacancies. All the vacancies might not be occupied by oxygen, so at the end a mixture of CdO and CdS with an excess of cadmium is obtained [66]. It is presumable that CdS could undergo a similar reaction under continuous UV exposure in air. Nevertheless, oxidation of metal sulfides is a very complex exothermal heterogeneous process that involves multi-step reactions, so a clear picture of the overall reaction is not straightforward [67].

A mechanism that could account for the observed effects is the following. Charge carriers resulting from light adsorption could be trapped at the surface defects because of the mismatched atomic scale topology of the CdS particles. The photoexcited electron could activate reaction with oxygen (either from the SiO_2 or from the air), leading to the formation of SO_2 , which would then be progressively desorbed, resulting in the gradual erosion and smoothing of the particle surface. The excess Cd at the surface could then bond to oxygen to form a CdO shell, which would effectively passivate the particle, leading to the observed enhanced PL. Some authors have in fact shown that the formation of a thin CdO shell by treating CdS nanoparticles with NaBH_4 , can indeed lead to an increase in the PL intensity [68].

4. Conclusions

CdS has been successfully infiltrated within the mesopores of ordered silica templates to obtain SiO_2/CdS nanocomposites, in which the CdS is forming a continuous network rather than isolated nanoparticles. Self-supported CdS structures have been observed upon removal of silica templates. The obtained PL spectra, particularly those of the SiO_2/CdS composites, consist of high-intensity emission broad peaks, covering the overall visible wavelength range. In the case of SBA-16 mesostructures, an irreversible photoactivation effect during light illumination is observed, which can be attributed to surface chemical reaction involving desorption of SO_2 and concomitant enrichment in Cd, which brings about passivation of particle surface, and thus result in an annihilation of surface traps.

We have shown that the fabrication of ordered nanocavity arrays able to accommodate a wide band-gap II–VI semiconductor material is an innovative strategy that could open up a vast range of opportunities for catalysis and photonics. Although the CSLM does not provide absolute PL values, it is a powerful tool to qualitatively study the PL properties of non-biological materials, being particularly well suited to assess the photoactivation effects in mesoporous SiO_2/CdS materials.

Acknowledgments

The authors wish to acknowledge the Spanish MINECO (MAT2011-27380-C02-01) and the Catalan DGR (2009-SGR-1292) for partial financial support. The authors also thank P. Garcia for his assistance during small-angle XRD experiments and the Servei

d'Anàlisi Química of the Universitat Autònoma de Barcelona for their technical support during the measurements of UV-VIS absorption spectra. M.D.B. acknowledges partial financial support from an ICREA-Academia Award.

Appendix A. Supplementary material

Compositional analysis (S1) of the materials, reproducibility of the multi-peak structure in the PL spectra (S2) and media files (S3 and S4). **Supplementary data associated with this article can be found, in the online version, at <http://dx.doi.org/10.1016/j.jcis.2013.06.022>.**

References

- [1] A.P. Alivisatos, *J. Phys. Chem. C* 100 (1996) 13226.
- [2] W. Chen, Y. Xu, Z. Lin, Z. Wang, L. Lin, *Solid State Comm.* 105 (1998) 129.
- [3] M. Bruchez, M. Moronne, P. Gin, S. Weiss, A.P. Alivisatos, *Science* 281 (1998) 2013.
- [4] I.L. Medintz, H.T. Uyeda, E.R. Goldman, H. Mattoussi, *Nature Mater.* 4 (2005) 435.
- [5] X.Q. Li, Y.W. Wu, D. Steel, D. Gammon, T.H. Stievater, D.S. Katzer, D. Park, C. Piermarocchi, L.J. Sam, *Science* 301 (2003) 809.
- [6] M.J. Bowers II, J.R. McBride, S.J. Rosenthal, *J. Am. Chem. Soc.* 127 (2005) 15378.
- [7] E.F. Schubert, J.K. Kim, H. Luo, J.-Q. Xi, *Rep. Prog. Phys.* 69 (2006) 3069.
- [8] S. Nizamoglu, E. Mutlugun, O. Akyuz, N.K. Perkgoz, H.V. Demir, L. Liebscher, S. Sapra, N. Gaponik, A. Eychmueller, *New J. Phys.* 10 (2008) 023026.
- [9] Y. Sun, N.C. Giebink, H. Kanno, B. Ma, M.E. Thompson, S.R. Forrest, *Nature* 440 (2006) 908.
- [10] S.F. Chichibu, A. Uedono, T. Onuma, B.A. Haskell, A. Chakraborty, T. Koyama, P.T. Fini, S. Keller, S.P. Denbaars, J.S. Speck, U.K. Mishra, S. Nakamura, S. Yamaguchi, S. Kamiyama, H. Amano, I. Akasaki, J. Han, T. Sota, *Nature Mater.* 5 (2006) 810.
- [11] P.O. Anikeeva, J.E. Halpert, M.G. Bawendi, V. Bulović, *Nano Lett.* 7 (2007) 2196.
- [12] M. Molaei, E.S. Iranizad, M. Marandi, N. Taghavinia, *AIP Adv.* 1 (2011) 012113.
- [13] L. Qu, X. Peng, *J. Am. Chem. Soc.* 124 (2002) 2049.
- [14] X. Gao, Y. Cui, R.M. Levenson, L.W.K. Chung, S. Nie, *Nature Biotechnol.* 22 (2004) 969.
- [15] S. Dembski, C. Graf, T. Kruger, U. Gbureck, A. Ewald, A. Bock, E. Ruhl, *Small* 4 (2008) 1516.
- [16] J.L. Vivero-Escoto, I.I. Slowing, B.G. Trewyn, V.S.-Y. Lin, *Small* 6 (2010) 1952.
- [17] D. Gerion, F. Pinaud, S.C. Williams, W.J. Parak, D. Zanchet, S. Weiss, A.P. Alivisatos, *J. Phys. Chem. B* 105 (2001) 8861.
- [18] H. Yang, P.H. Holloway, *Appl. Phys. Lett.* 82 (2003) 1965.
- [19] A.Y. Nazzal, L. Qu, X. Peng, M. Xiao, *Nano Lett.* 3 (2003) 819.
- [20] S.R. Cordero, P.J. Carson, R.A. Estabrook, G.F. Strouse, S.K. Buratto, *J. Phys. Chem. B* 104 (2000) 12137.
- [21] K. Sato, S. Kojima, S. Hattori, T. Chiba, K. Ueda-Sarson, T. Torimoto, Y. Tachibana, S. Kuwabata, *Nanotechnology* 18 (2007) 465702.
- [22] L. Hu, H. Wu, L. Du, H. Ge, X. Chen, N. Dai, *Nanotechnology* 22 (2011) 125202.
- [23] J.W.M. Chon, P. Zijlstra, M. Gu, J. van Embden, P. Mulvaney, *Appl. Phys. Lett.* 85 (2004) 5514.
- [24] T. Moto, K. Maruyama, H. Endo, *J. Phys. Condens. Matter* 4 (1992) 5653.
- [25] T. Zhai, X. Fang, L. Li, Y. Bando, D. Golberg, *Nanoscale* 2 (2010) 168.
- [26] E.D. Sone, E.R. Zubarev, S.I. Stupp, *Angew. Chem. Int. Ed.* 41 (2002) 1705.
- [27] C. Delerue, G. Allan, M. Lannoo, *Phys. Rev. B* 48 (1993) 11024.
- [28] Y. Shi, Y. Wan, D. Zhao, *Chem. Soc. Rev.* 40 (2011) 3854.
- [29] M.G. Kanatzidis, *Adv. Mater.* 19 (2007) 1165.
- [30] W.-M. Zhang, N. Li, D.-H. Tang, Y.-Y. Wang, *Micro. Meso. Mater.* 143 (2011) 249.
- [31] P.V. Braun, P. Osenar, S.I. Stupp, *Nature* 380 (1996) 325.
- [32] P.V. Braun, P. Osenar, V. Tohver, S.B. Kennedy, S.I. Stupp, *J. Am. Chem. Soc.* 121 (1999) 7302.
- [33] J.L. Mohanan, I.U. Arachchige, S.L. Brock, *Science* 307 (2005) 397.
- [34] X. Cao, N. Wang, X. Kim, *Electrochim. Acta* 56 (2011) 9504.
- [35] N. Herron, Y. Wang, M.M. Eddy, G.D. Stucky, D.E. Cox, K. Moller, T. Bein, *J. Am. Chem. Soc.* 111 (1989) 530.
- [36] G.D. Stucky, J.E. Macdougall, *Science* 247 (1990) 669.
- [37] J.-L. Shi, *J. Mater. Chem.* 14 (2004) 795.
- [38] M. Yosef, A.K. Schaper, M. Fröba, S. Schlecht, *Inorg. Chem.* 44 (2005) 5890.
- [39] T. Hirai, H. Okubo, I. Komasaawa, *J. Phys. Chem. B* 103 (1999) 4228.
- [40] W. Xu, Y. Liao, D.L. Akins, *J. Phys. Chem. B* 106 (2002) 11127.
- [41] L. Fernández, N. Garro, J. El Haskouri, M. Pérez-Cabero, J. Álvarez-Rodríguez, J. Latorre, C. Guillem, A. Beltrán, D. Beltrán, P. Amorós, *Nanotechnology* 19 (2008) 225603.
- [42] T. Hirai, H. Okubo, I. Komasaawa, *J. Colloid Interface Sci.* 235 (2001) 358.
- [43] T. Hirai, M. Nanba, I. Komasaawa, *J. Colloid Interface Sci.* 268 (2003) 394.
- [44] F. Gao, Q.Y. Lu, D.Y. Zhao, *Adv. Mater.* 15 (2003) 739.
- [45] X.Y. Liu, B.Z. Tian, C.Z. Yu, B. Tu, Z. Liu, O. Terasaki, D.Y. Zhao, *Chem. Lett.* 32 (2003) 824.
- [46] N. Yuan, G. Cheng, Y. An, Z. Du, S. Wu, *Nanoscale Res. Lett.* 4 (2009) 414.

- [47] A.V. Kouzema, M. Fröba, L. Chen, P.J. Klar, W. Heimbrot, *Adv. Funct. Mater.* 15 (2005) 168.
- [48] M. Pauchard, S. Huber, R. Méallet-Renault, H. Maas, R. Pansu, G. Calzaferri, *Angew. Chem. Int. Ed.* 40 (2001) 2839.
- [49] N. Gartmann, D. Brühwiler, *Angew. Chem. Int. Ed.* 48 (2009) 6354.
- [50] M.A. Olshavsky, H.R. Allcock, *Chem. Mater.* 9 (1997) 1367.
- [51] D.Y. Zhao, Q.S. Huo, J.L. Feng, B.F. Chmelka, G.D. Stucky, *J. Am. Chem. Soc.* 120 (1998) 6024.
- [52] L. Lutterotti, P. Scardi, *J. Appl. Crystallogr.* 23 (1990) 246.
- [53] K. Jiao, B. Zhang, B. Yue, Y. Ren, S. Liu, S. Yan, C. Dickinson, W. Zhou, H. He, *Chem. Comm.* (2005) 5618.
- [54] R. Xu, Y. Wang, G. Jia, W. Xu, S. Liang, D. Yin, *J. Crystal Growth* 299 (2007) 28.
- [55] C.B. Murray, D.J. Norris, M.G. Bawendi, *J. Am. Chem. Soc.* 115 (1993) 8706.
- [56] Y. Wang, Z. Tang, M.A. Correa-Duarte, I. Pastoriza-Santos, M. Giersig, N.A. Kotov, L.M. Liz-Marzán, *J. Phys. Chem. B* 108 (2004) 15461.
- [57] W. Chen, Z. Wang, Z. Lin, L. Lin, *Appl. Phys. Lett.* 70 (1997) 1465.
- [58] M.A. Correa-Duarte, M. Giersig, L.M. Liz-Marzán, *Chem. Phys. Lett.* 286 (1998) 497.
- [59] W. Zhang, H.-R. Lee, *J. Photochem. Photobiol. A: Chem.* 218 (2011) 1.
- [60] Y.K. Xu, S. Adachi, *J. Appl. Phys.* 107 (2010) 123520.
- [61] N.S. Averkiev, V.M. Asnin, A.B. Churilov, I.I. Markov, N.E. Mokrousov, A.Y. Silov, V.I. Stepanov, *JETP Lett.* 55 (1992) 657.
- [62] H. Koyama, *J. Appl. Electrochem.* 36 (2006) 999.
- [63] H. Elhouichet, M. Oueslati, *Appl. Surf. Sci.* 191 (2002) 11.
- [64] W.G.J.H.M. van Sark, P.L.T.M. Frederix, D.J. Van den Heuvel, H.C. Gerritsen, *J. Phys. Chem. B* 105 (2001) 8281.
- [65] L. Manna, E.C. Scher, *J. Am. Chem. Soc.* 124 (2002) 7136.
- [66] A.J. Haider, A.M. Mousa, S.M.H. Al-Jawad, *J. Semicond. Technol. Sci.* 8 (2008) 326.
- [67] R.I. Dimitrov, N. Moldovanska, I.K. Bonev, *Thermochim. Acta* 385 (2002) 41.
- [68] E. Jang, S. Jun, Y. Chung, L. Pu, *J. Phys. Chem. B* 108 (2004) 4597.